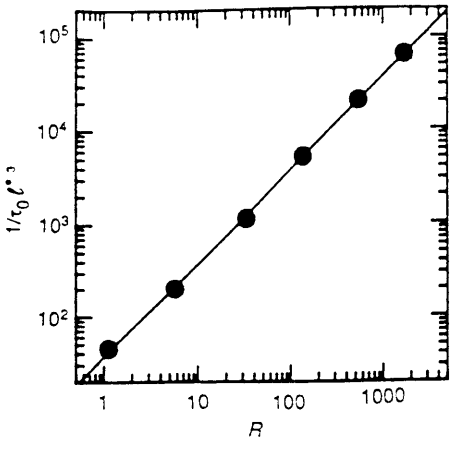

Fig. 5. The quantity $1/\tau_0\ell^{*3}$ versus the rate of rearrangement events per unit volume; we estimated the latter by viewing surface bubbles with a microscope. Both quantities are in units of s^{-1} cm^{-3}. The solid line is the best fit to $1/\tau_0\ell^{*3} \propto R$.

whereupon its length is suddenly changed and the phase is totally randomized. Thus, $g_1^s(\tau)$ is an ensemble average of the fraction of paths of length s that have not been randomized since time $\tau = 0$. If rearrangement events of a single size r occur randomly at rate R per unit volume, then $g_1^s(\tau) = e^{-\gamma_s \tau}$. The decay rate γ_s depends on the likelihood of a rearrangement event occurring within the path and so increases with the product of R and the path volume, $s\ell^{*2}$, where ℓ^* is the shortest meaningful length scale for a diffusive light path. Also, γ_s must increase with r^3/ℓ^{*3}, because larger events will affect more light paths. We therefore have $\gamma_s \approx R(s\ell^{*2})(r^3/\ell^{*3})$; comparison with Eq. 5 gives $\tau_0^{-1} \approx Rr^3$. Physically, τ_0 reflects the average time interval between rearrangement events at any single location in the foam.

To test this model, in Fig. 5 we compare $1/\tau_0\ell^{*3}$, measured by DWS, with R, estimated from the rate of rearrangements at the foam surface. Provided the average event size r scales with bubble size, our model predicts $1/\tau_0\ell^{*3} \propto R$. As the foam ages, both quantities decrease by many orders of magnitude, and Fig. 5 demonstrates a linear relation over the full range. The result, $1/\tau_0\ell^{*3} = (35 \pm 10)R$ (*10*), implies that the average event size scales with bubble size and is on the order of ten bubbles in diameter. This is in excellent agreement with our microscope observations of r, confirming the validity of our model for DWS.

In contrast to traditional dynamic light-scattering techniques, which probe continuous random movements, this form of DWS probes events that are temporally intermittent, large in scale, and spatially localized. Studying the time evolution of the foam, we find that $R \sim t^{-\gamma}$ with $\gamma = 2.0 \pm 0.1$ (*10*, *11*). The origin, scaling behavior, and consequences of these rearrangement events have not yet been considered. Presumably, as the foam coarsens and packing conditions change, local stress differences accumulate until a critical value is reached and a rearrangement event occurs. This process must also play an essential role in the relaxation of applied stresses and therefore should provide important microscopic information about the macroscopic rheological behavior of foams. In general, rearrangement events may vary considerably with the nature of the foam, particularly with the volume fraction of liquid and with the prevalence of bubble coalescence. However, the simplicity and convenience of these multiple light-scattering techniques should enable these and other important fundamental properties of a wide variety of foams to be studied.

REFERENCES AND NOTES

1. I. H. Aubert, A. M. Kraynik, P. B. Rand, *Sci. Am.* 254, 74 (May 1986).
2. A. J. Wilson, Ed., *Foams: Physics, Chemistry, and Structure* (Springer-Verlag, New York, 1989).
3. H. C. Cheng and T. E. Natan, in *Encyclopedia of Fluid Mechanics*, vol. 3, *Gas Liquid Flow*, N. P. Cheremisinoff, Ed. (Gulf, Houston, 1986).
4. A. M. Kraynik, *Annu. Rev. Fluid Mech.* 20, 325 (1988).
5. N. O. Clark and M. Blackman, *Trans. Faraday Soc.* 44, 7 (1948); S. Ross and M. J. Cutillas, *J. Phys. Chem.* 59, 863 (1955).
6. Gillette Foamy Regular (Gillette Company, Box 61, Boston, MA 02199).
7. A. Ishimaru, *Wave Propagation and Scattering in Random Media* (Academic Press, New York, 1978), vol. 1.
8. P. E. Wolf, G. Maret, E. Akkermans, R. Maynard, *J. Phys. (Paris)* 49, 63 (1988).
9. W. W. Mullins, *J. Appl. Phys.* 59, 1341 (1986).
10. The quoted error reflects our estimate of the systematic uncertainties in the light-scattering measurements and in the estimate of bulk foam properties obtained by viewing surface bubbles.
11. D. J. Durian, D. A. Weitz, D. J. Pine, in preparation.
12. G. Maret and P. E. Wolf, *Z. Phys. B* 65, 409 (1987).
13. D. J. Pine, D. A. Weitz, J. X. Zhu, E. Herbolzheimer, *J. Phys. (Paris)* 51, 2101 (1990).
14. B. J. Berne and R. Pecora, *Dynamic Light Scattering: With Applications to Chemistry, Biology, and Physics* (Wiley, New York, 1976).
15. We generalize equation 3.5 of (*13*) to include the effect of absorption.
16. D. Weire and N. Rivier, *Contemp. Phys.* 25, 59 (1984).
17. J. A. Glazier, S. P. Gross, J. Stavans, *Phys. Rev. A* 36, 306 (1987).

18. We thank T. A. Witten and P. M. Chaikin for suggestions and the deckmen for their help.

16 November 1990; accepted 8 February 1991

Molecular Self-Assembly of Two-Terminal, Voltammetric Microsensors with Internal References

JAMES J. HICKMAN, DAVID OFER, PAUL E. LAIBINIS, GEORGE M. WHITESIDES, MARK S. WRIGHTON*

Self-assembly of a ferrocenyl thiol and a quinone thiol onto Au microelectrodes forms the basis for a new microsensor concept: a two-terminal, voltammetric microsensor with reference and sensor functions on the same electrode. The detection is based on measurement of the potential difference of current peaks for oxidation and reduction of the reference (ferrocene) and indicator (quinone) in aqueous electrolyte in a two-terminal, linear sweep voltammogram in which a counterelectrode of relatively large surface area is used. The quinone has a half-wave potential, $E_{1/2}$, that is pH-sensitive and can be used as a pH indicator; the ferrocene center has an $E_{1/2}$ that is a pH-insensitive reference. The key advantages are that such sensors require no separate reference electrode and function as long as current peaks can be located for reference and indicator molecules.

WE REPORT PROOF-OF-CONCEPT results demonstrating a new approach to electrochemical sensors: two-terminal, voltammetric microsensors with internal references (Fig. 1). Detection is accomplished by measurement of the potential difference, ΔE, associated with current peaks for oxidation (or reduction) of microelectrode-confined redox reagents, where the magnitude of ΔE can be related to the concentration of analyte. One of the electrode-bound reagents has an electrochemical response that is insensitive to variations in the medium and serves as the reference. At least one of the electrode-bound reagents is chemically sensitive and serves as the indicator. Current peaks for oxidation or reduction of the reference and indicator are determined from two-terminal, linear sweep voltammograms in which a counterelectrode is used that has an area

J. J. Hickman, D. Ofer, M. S. Wrighton, Department of Chemistry, Massachusetts Institute of Technology, Cambridge, MA 02139. P. E. Laibinis and G. M. Whitesides, Department of Chemistry, Harvard University, Cambridge, MA 02138.

*To whom correspondence should be addressed.

much larger than that of the sensor electrode. A counterelectrode with relatively large surface area is needed so that the linear sweep of applied voltage will yield only a change in potential of the sensor electrode. For example, if the counter electrode is 10^3 times as large as the sensor electrode, the counterelectrode potential moves only ~1 mV on application of a 1-V potential difference. The key advantage of our new device is that it does not require a reference electrode because the indicator and reference molecules are both on the sensor electrode. A second advantage is that the sensor function is based on peak-to-peak separations, ΔE, rather than on peak amplitudes. Accordingly, the sensor can be useful as long as peaks can be located, even when slow decomposition of the electrode-bound reagents occurs.

Realization of a two-terminal, voltammetric microsensor depends on discovery of viable reference and indicator molecules that can be confined to electrode surfaces. Our system is prepared by self-assembly of two redox-active molecules on Au microelectrodes by adsorption of the RSH group on gold (as thiolate, RS^-Au^+, where R is an alkyl group) (Fig. 1) (*1–5*). The reference molecule is a ferrocene (Fc), a redox center with a chemically insensitive formal potential (*6*). The indicator molecule is a hydroquinone (QH_2), which has a pH-dependent redox potential (*7*). Quinone thiols (*8, 9*) and ferrocene thiols (*10, 11*) have been attached separately to Au electrodes.

One can modify Au microelectrodes (*12*) (~10^3 μm^2) or Au macroelectrodes (~1 cm^2) with QH_2 (*13*) or Fc (*11*) by dipping the Au into solutions containing one or both of the thiol reagents (*14*). Cyclic voltammograms for Au macroelectrodes modified with pure Fc, QH_2, or a combination of Fc and QH_2, are shown in Fig. 2. The electrochemical response is persistent and consistent with about one monolayer of redox-active molecules. Coverages determined from integration of the current-voltage curves are 3×10^{-10} to 5×10^{-10} mol/cm^2. The combination of QH_2 and Fc on the Au yields an electrochemical response expected from the presence of both redox systems. The electrochemical response for a Au microelectrode derivatized with QH_2 and Fc at two values of pH (Fig. 3) indicates that the redox potential for the Fc^+-Fc system (Eq. 1) is pH-insensitive, whereas the redox response for the Q-QH_2 system (Eq. 2) depends on pH.

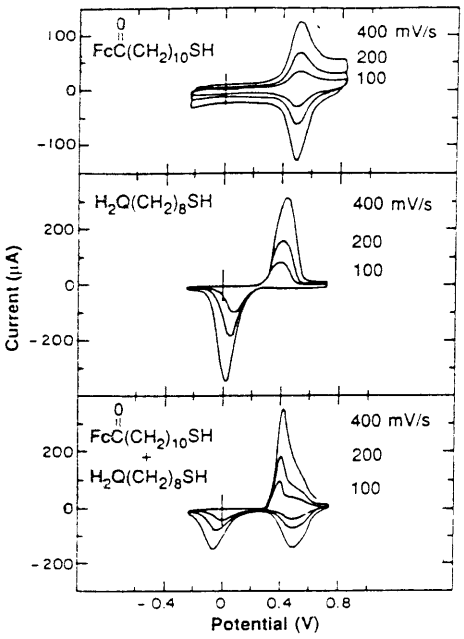

Fig. 2. Cyclic voltammetry at three scan rates for Au macroelectrodes in 1.0 M $NaClO_4$ at pH 1.5 buffer (phosphate) derivatized with only acyl Fc thiol (5.2×10^{-10} mol/cm^2) (top); only Q thiol (5.6×10^{-10} mol/cm^2) (middle); and a mixture of the acyl Fc thiol and Q thiol at 3.9×10^{-10} mol/cm^2 and 1.7×10^{-10} mol/cm^2, respectively (bottom).

$$Fc^+ + e^- \rightleftarrows Fc \quad (1)$$

$$Q + 2e^- + 2H^+ \rightleftarrows QH_2 \quad (2)$$

When the Au microelectrode is run as the sensor electrode in a two-terminal device (~1 cm^2 Pt counter electrode), the voltammograms are superimposable on the curves shown in Fig. 3, where a saturated calomel (SCE) reference electrode was used. The microelectrodes show a somewhat smaller potential window than macroelectrodes in the aqueous electrolytes. This disadvantage is, however, compensated for by the fact that microelectrodes modified with a monolayer of reference and indicator molecules minimize the charge passed in effecting the movement of potential of the sensor electrode. Thus, both the size of the counter electrode and the perturbation of the solution interrogated can be minimized.

The surface-confined Fc^+-Fc system be-

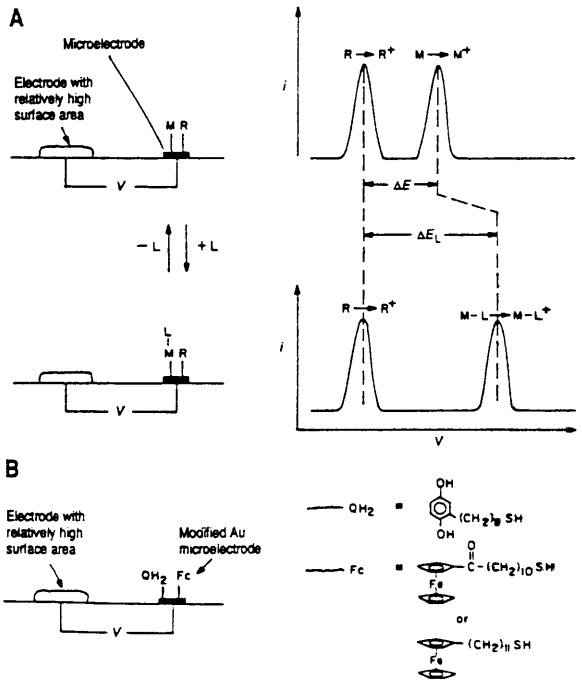

Fig. 1. (**A**) Concept of a two-terminal, voltammetric microsensor showing idealized response to a species L that binds to the indicator molecule M. The linear sweep voltammograms reveal a difference between the current peaks for oxidizing the reference molecule, R, and M or M-L, depending on the presence of L. (**B**) System designed for measuring pH where the Fc thiol can serve as a reference, R, and the QH_2 thiol can serve as an indicator, M, for pH.

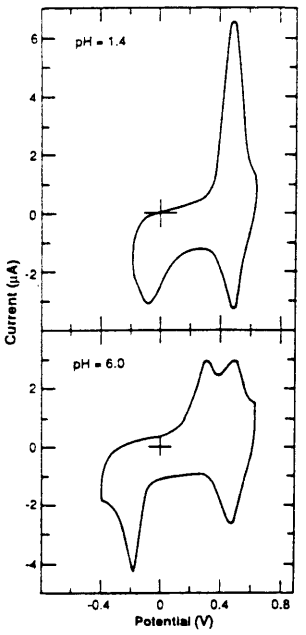

Fig. 3. Cyclic voltammetry (500 mV/s) of Au microelectrodes derivatized with a mixture of acyl Fc thiol and Q thiol at pH 1.4 and pH 6.0. The solutions used were phosphate buffers in 1.0 M $NaClO_4$ base electrolyte; an SCE reference electrode was used.

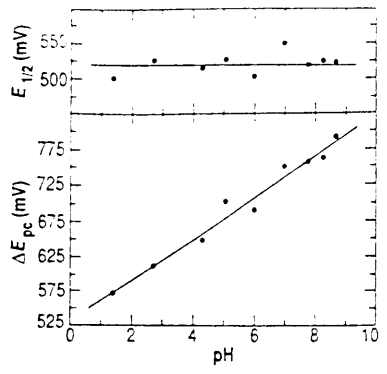

Fig. 4. Plot of $E_{1/2}$ versus SCE for the surface-confined Fc thiol versus pH (top) and plot of difference in cathodic current peak for surface-confined acyl Fc^+ and Q versus pH from two-terminal, voltammetric scans. All data are from voltammograms recorded at 500 mV/s in 1.0 M $NaClO_4$ in buffered solution.

haves ideally (*15*) at all values of pH investigated (0 to 10). The surface-confined Q-QH_2 system is not ideal in that there is a large difference in the potential for the anodic and cathodic current peaks. Such behavior is well documented for other quinones (*9, 16*). Although the Q-QH_2 system is not ideal, the effect of pH on the electrochemical response of Q-QH_2 is reproducible. Both the anodic and cathodic current peaks for the Q-QH_2 system shift to more positive potentials at lower pH. The $E_{1/2}$ of the surface-confined Fc^+-Fc system is pH-insensitive and the potential difference between the cathodic current peaks, ΔE_{pc}, is pH-dependent for the processes shown in Eqs. 1 and 2 (Fig. 4). The linear response to the solution pH forms the basis for a pH sensor system where the Fc^+-Fc serves as the reference and the Q-QH_2 serves as the indicator (Fig. 1).

These results illustrate our concept of a two-terminal microelectrochemical sensor. Study of electrodes modified with Q and 11-ferrocenylundecanethiol, $Fc(CH_2)_{11}SH$ (*10*), and subsequently examined in highly acidic media establishes a possible application of our new concept. The electrochemical response of a derivatized Au macroelectrode in aqueous media containing different concentrations of $HClO_4$ is illustrated in Fig. 5. The electrochemical response of the redox molecules persists even in 10 M $HClO_4$. Note that the response for the Q-QH_2 system moves from −0.5 V negative (pH = 11) of the Fc to −0.5 V positive (10 M $HClO_4$) of Fc for the media used. Measuring H^+ activity in highly acidic media is thus possible with the electrode modified with both Q and Fc $(CH_2)_{11}SH$. Earlier work has established the constancy of the redox potential of a surface-confined Fc at very high H^+ activity (*17*), justifying our use of the Fc as an internal reference in such media. In applications, locating peak positions in linear sweep voltammetry can be improved with the use of derivative voltammetry (*18*). The linear sweep voltammograms and the first derivatives in 0.1 M and 3 M $HClO_4$ illustrate the use of the derivatives to establish the differences in the peak positions for the oxidation of the Fc and the QH_2 centers confined to a Au electrode (Fig. 6).

The proof-of-concept microsensor system described here can be easily extended by use of other specific indicator molecules. Monolayer redox reagents and microelectrodes are not required, but their use has the advantage that very small amounts of charge are involved in detection. The self-assembly of thiol reagents provides a reproducible method, applicable to many chemical functionalities (*1–5, 8–11*), for assembly of device-active materials, but there are a large number of other electrode modification techniques that can be useful (*15*). Au electrodes derivatized with thiol reagents are robust, but long-term durability is an issue in many sensor applications. Sensor electrodes described have been used intermittently over a period of several weeks with reproducible response to variation in pH. At least the two-terminal, voltammetric microsensor is self-assessing in that failure of the device-active materials is revealed by an inability to detect current peaks. It should be possible to devise multiple-response, two-terminal microsensors by incorporation of more than one indicator molecule.

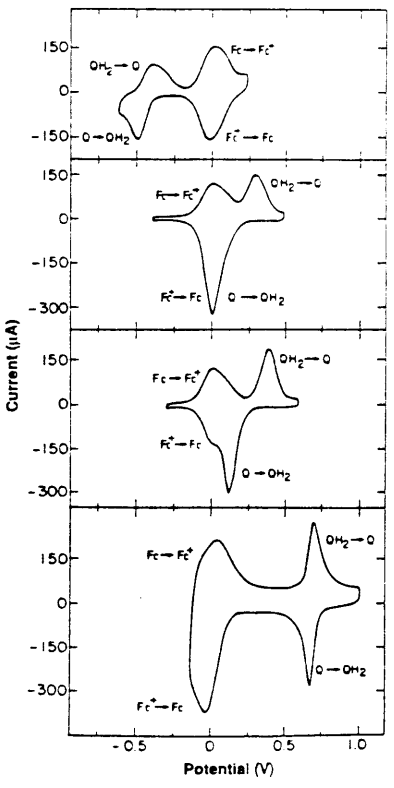

Fig. 5. Cyclic voltammetry (500 mV/s) for a Au macroelectrode derivatized with alkyl Fc thiol and Q thiol in (from top to bottom) 1.0 M $NaClO_4$ buffered to pH 11 with phosphate (0.05 M Na_2HPO_4 and 0.05 M Na_3PO_4); 0.1 M $HClO_4$; 1.0 M $HClO_4$; 10 M $HClO_4$. The reference is taken to be the average position of the oxidation and reduction waves for the ferrocene system.

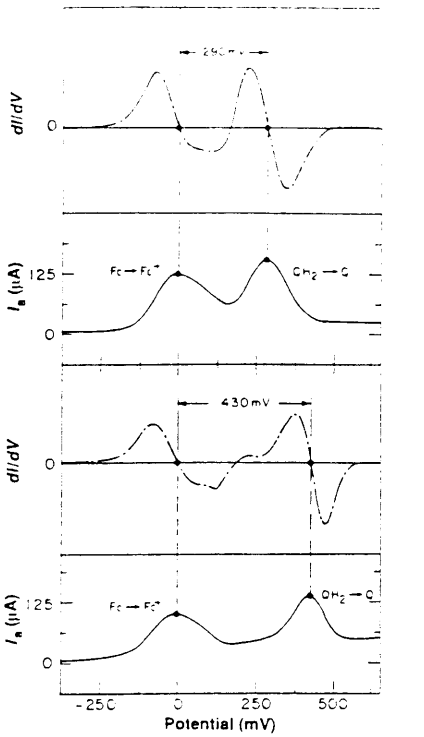

Fig. 6. Linear sweep voltammograms (500 mV/s) and their first derivatives for oxidation of alkyl Fc thiol and QH_2 thiol confined to a Au macroelectrode. Top two panels, 0.1 M $HClO_4$. Bottom two panels, 3 M $HClO_4$. The potential scale is relative to the Fc oxidation wave.

REFERENCES AND NOTES

1. R. G. Nuzzo and D. L. Allara, *J. Am. Chem. Soc.* **105**, 4481 (1983).
2. A. P. Brown, C. Koval, F. C. Anson, *J. Electroanal. Chem.* **72**, 379 (1976); C. D. Bain and G. M. Whitesides, *J. Am. Chem. Soc.* **110**, 5897 (1988); M. D. Porter, T. B. Bright, D. L. Allara, C. E. D. Chidsey, *ibid.* **108**, 3559 (1986).
3. C. D. Bain and G. M. Whitesides, *Science* **240**, 62 (1988); *J. Am. Chem. Soc.* **110**, 3665 and 6561 (1988); *Angew. Chem. Int. Ed. Engl.* **101**, 522 (1989); G. M. Whitesides and P. E. Laibinis, *Langmuir* **6**, 87 (1990).
4. C. D. Bain *et al.*, *J. Am. Chem. Soc.* **111**, 321 (1989).
5. D. L. Allara and R. G. Nuzzo, *Langmuir* **1**, 45 and 52 (1985).
6. P. J. Peerce and A. J. Bard, *J. Electroanal. Chem.* **108**, 121 (1980); T. A. Modro, K. Yates, J. Janata, *J. Am. Chem. Soc.* **97**, 1492 (1975), and references therein.
7. A. Streitwieser and C. H. Heathcock, *Introduction to Organic Chemistry* (Macmillan, New York, ed. 2, 1981), pp. 1014–1020.
8. D. A. Stern *et al.*, *J. Am. Chem. Soc.* **110**, 4885 (1988).
9. A. T. Hubbard, *Chem. Rev.* **88**, 633 (1988).
10. C. E. D. Chidsey, C. R. Bertozzi, T. M. Putvinski, A. M. Mujsce, *J. Am. Chem. Soc.* **112**, 4301 (1990).

11. J. J. Hickman, D. Ofer, P. E. Laibinis, G. M. Whitesides, M. S. Wrighton, *ibid.*, 113, 1128 (1991).
12. The microelectrode arrays consist of eight wires (~2 μm wide by ~50 μm long by ~0.1 μm thick) separated from each other by ~1.4 μm on a flat Si_3N_4-coated Si substrate [G. P. Kittlesen, H. S. White, M. S. Wrighton, *J. Am. Chem. Soc.* 106, 7389 (1984)]. The leads connecting the microelectrodes to macroscopic bonding pads were encapsulated under an additional layer of Si_3N_4. The electrodes were electrochemically plated with an additional layer of fresh Au and cleaned by sonication and then further cleaned in an O_2 plasma for 8 min, after which oxide was reduced by treatment for 2 min in an H_2 plasma. All eight microelectrodes were derivatized and used as one sensor electrode of $\sim 10^3$ μm² area.
13. Preparation of 2-(8-mercaptooctyl) hydroquinone involved several steps: 1,4-dimethoxy-benzene was deprotonated with *n*-butyllithium and added to excess 1,8-dibromooctane; vacuum distillation afforded 2-(8-bromooctyl)-1,4-dimethoxybenzene; demethylation was accomplished in quantitative yield with BBr_3; the bromide was displaced by thioacetate; and subsequent hydrolysis under acidic conditions yielded the thiol, which was purified by chromatography. Materials were characterized by ^1H NMR spectroscopy. Analysis: calculated (found) for $C_{14}H_{22}O_2S$: C, 66.10 (66.21); H, 8.72 (8.58); and S, 12.60 (12.57).
14. The molecules were self-assembled onto Au surfaces by placement of the Au into ~1 mM solutions of Fc or QH_2 in tetrahydrofuran (THF) or 1:1 ethanol: hexane. Mixtures of Fc and QH_2 were self-assembled onto Au from a 2:1 QH_2:Fc mixture in THF or in 1:1 ethanol:hexane at a total thiol concentration of ~1 mM. All derivatizations were carried out under Ar at 25°C for ~24 hours.
15. R. W. Murray, in *Electroanalytical Chemistry*, A. J. Bard, Ed. (Dekker, New York, 1984), vol. 13, pp. 191–368, and references therein.
16. E. Laviron, *J. Electroanal. Chem.* 146, 15 (1983); *ibid.* 164, 213 (1984).
17. A. B. Fischer, thesis, Massachusetts Institute of Technology, Cambridge (1981).
18. V. D. Parker, in *Electroanalytical Chemistry*, A. J. Bard, Ed. (Dekker, New York, 1986), vol. 14, pp. 1–111.
19. We thank the Office of Naval Research and the Defense Advanced Research Projects Agency for partial support of this research. We acknowledge use of XPS and Auger facilities acquired through the joint Harvard/MIT University Research Initiative funded by the Defense Advanced Research Projects Agency.

6 December 1990; accepted 21 February 1991

Three-Dimensional Readout of Flash X-ray Images of Living Sperm in Water by Atomic-Force Microscopy

T. TOMIE,* H. SHIMIZU, T. MAJIMA, M. YAMADA, T. KANAYAMA, H. KONDO, M. YANO, M. ONO

The imaging of living specimens in water by x-ray microscopy can be greatly enhanced with the use of an intense flash x-ray source and sophisticated technologies for reading x-ray images. A subpicosecond x-ray pulse from a laser-produced plasma was used to record the x-ray image of living sea urchin sperm in an x-ray resist. The resist relief was visualized at high resolution by atomic-force microscopy. Internal structure of the sperm head was evident, and the carbon density in a flagellum was estimated from the relief height.

X-RAY MICROSCOPY (XRM) HAS many potential advantages over electron microscopies (EMs) (*1*). The most favored application is the observation of living cells in water with the use of x-rays in the so-called water-window wavelength region (2.32 to 4.37 nm). Although there have been many synchrotron-radiation XRM studies (*2*) with an exposure time longer than a few seconds, flash exposure is essential for high-resolution imaging (*3*). Although a 100-ns x-ray pulse was used in the first experiment of flash XRM of specimen in water (*4*), the maximum exposure time for high-resolution imaging is considered to be shorter than 1 ns, as discussed below. Such a short duration flash x-ray is currently available only from a laser-produced plasma.

Along with the difficulty of obtaining an intense flash x-ray source, the other major problem in flash XRM has been reading the x-ray images. High-resolution flash XRM is possible at present only in contact XRM, in which the x-ray shadow of a specimen is recorded in the closely contacted x-ray resist. The magnification of the image is achieved in the examination stage of the recorded profile. In the examination by EMs, radiation damage by the electron beam of the resist surface or a replica of the resist relief has been a serious problem (*5*). We have used atomic-force microscopy (AFM) (*6*) because the relief on a nonconducting resist surface can be examined directly without coating or making a replica. In microscopy, one wants to observe both thin and thick features in the same image, and the recording material should have a large dynamic range, contrary to the case of lithography, in which an on-off pattern is required. When a dynamic range is large, the contrast of the image is inevitably low. AFM is a good technique for examining low-contrast topography. Moreover, the relief height can be measured with high precision, which allows us to discuss the density of specimens quantitatively. We report the use of AFM in contact XRM in imaging sea urchin sperm.

After a detailed study of the laser-plasma x-ray source (*7*), we succeeded in obtaining one-shot x-ray image of specimens in water by using a low-energy (2-J) laser pulse (*8*) (Fig. 1). The major concern in using a laser-plasma x-ray source was the effect of ultraviolet (UV) emission and debris from the plasma (*9*). We confirmed experimentally that the contribution of UV emission to resist exposure was negligible. Although the 0.1-μm-thick silicon nitride (Si_3N_4) membrane used as an x-ray window was broken after the x-ray exposure, the debris did not reach the resist surface when a specimen in water was imaged. The water between the membrane and the resist protected the resist surface from the debris. The specimen was the sperm of a sea urchin *Anthocidaris crassisspina* in semen solution. The undiluted semen was stored at 4°C. For the observation, the semen was diluted with a one-quarter volume of artificial seawater. A drop of the diluted semen was sandwiched between the Si_3N_4 membrane and a polymethylmethacrylate (PMMA) x-ray resist. The laser plasma was produced by a frequency-doubled glass laser pulse (500 ps, 2 J). The specimen was placed 6 mm from the x-ray source. The x-ray energy density on the resist was 5 to 10 mJ/cm². The main contri-

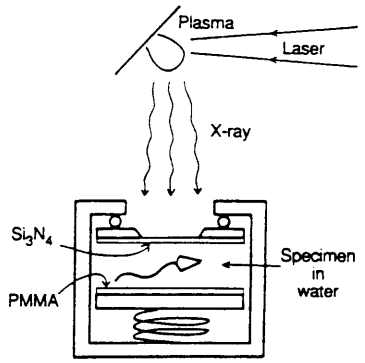

Fig. 1. Experimental configuration. A silicon nitride membrane of 0.1-μm thickness supported on a silicon wafer was used as an x-ray window. The membrane maintained the pressure difference between the vacuum region for the x-ray generation and the atmospheric specimen environment. The x-ray image is recorded in PMMA x-ray resist of 0.5-μm thickness spun on another silicon wafer. The separation between the membrane and the resist was 3 μm and was estimated from the x-ray transmission through water. The minimum separation is limited by the flatness of wafers.

T. Tomie, H. Shimizu, T. Majima, M. Yamada, T. Kanayama, M. Yano, M. Ono, Electrotechnical Laboratory, Tsukuba, Ibaraki, 305 Japan.
H. Kondo, Nikon Corporation, Tsukuba Laboratory, Tsukuba, Ibaraki, 300-26 Japan.

*To whom correspondence should be addressed.